An Experimental Flow Field Study of a Bio-inspired Corrugated Wing at Low Reynolds Number

Y. D. DWIVEDI*,[1], Y. B. SUDHIR SASTRY[1]

*Corresponding Author
[1]Department of Aeronautical Engineering, Institute of Aeronautical Engineering, Dundigal, Hyderabad, 500043, Telangana, India,
yddwivedi@gmail.com*, sudhirsastry.yb@iare.ac.in

DOI: 10.13111/2066-8201.2019.11.3.5

Received: 05 July 2019/ Accepted: 13 August 2019/ Published: September 2019

Abstract: *The present paper examined experimentally the glide flight flow visualization and boundary layers of a bio-inspired corrugated dragonfly wing performing a comparison with the results obtained with a flat plate, at low to moderate range of chord Reynolds numbers. The experimental work is performed in an open-end low speed subsonic wind tunnel at different angles of attack ranging from 0 to 12^0 and Reynolds number 2.25×10^5. The boundary layer measurements were done at a fixed chord location (0.7 x/c) and three different semi span locations such as 30%, 60% and 90% of the wing's semi span from the right side of the longitudinal axis of the wing. The flow patterns were visualized by using colored tufts, placed at different span locations. The flow reversal was observed at selected Reynolds numbers and angles of attack only. The boundary layer measurements demonstrated that there exists a clear distinction on the pressure and velocity parameters in all the three tested locations on both types of the wings. The corrugated wing showed significant delay in stall and flow separation compared with the flat plate. The visualization of flow in both wings showed that there subsists a spanwise flow moving from wing tip to root, indicating three dimensional natures of airflows.*

Key Words: *bio-inspired corrugation, boundary layer, flow reversal, spanwise flow, low Reynolds number*

1. INTRODUCTION

Insects, such as the dragonflies (*Sympetrum flaveolum*) are unique in their extreme aerodynamic performances like manoeuvrability, low noise signature, gliding ability, hovering capability, and high agility making them the perfect insect to replicate for micro air vehicles (MAVs) [1]. Dragonflies use flapping wings and stay aloft for longer duration without expending own energy, because of the gliding mode. Thus, the gliding feature of a dragonfly is a much desired aerodynamic performance which could be incorporated into the MAVs in terms of power saving capabilities. A number of studies [2-8] have been carried out to assess the flight performance of the insect wings by assimilating them with flat piece, formed by folding the wings membranes into V-shaped grooves. The corrugated wing configuration re-enforces wing stiffness in the spanwise direction also allowing torsion and enhancing the wing camber [9 and 10]. Morphological studies [11 and 12], revealed that the natural flyers are able to vary the corrugated pattern of the wing in both chordwise and spanwise directions. At the first look, it appears that the irregular geometry (zig-zag) of the corrugated wing promises poor aerodynamic performance in terms of low lift and high drag

or called less L/D ratio. Surprisingly, both experimental and computational studies [13-17] conducted on corrugated dragonfly wing models have shown consistently that the corrugations do not significantly increase drag during wing gliding. The reduction in the overall drag of the irregular corrugation is due to the negative viscous drag produced by the re-circulating fluids trapped inside the corrugated grooves [12 and 18]. However, there are many deliberations on the aerodynamic advantages of corrugations during gliding. Early experiments [13 and 14] on the corrugated airfoils confirmed that the corrugated wing has no more aerodynamic importance over its smooth airfoil. These experimental works were performed at a Reynolds number more than 10^4, this is one order of magnitude higher than that measured for the real dragonflies ($Re=10^3$). Some experiments [19] conducted at even higher Reynolds numbers; the result showed that the corrugation of airfoil produces improved aerodynamic performance by generating higher lift, and discouraging flow separation and airfoil stall. It is noted [20 and 21], that even for turbulent flows the corrugated grooves can strongly affect and induce spanwise flow. On the other hand, past computational studies conducted over a range of angle of attack (0–40°) as well as Reynolds numbers (10^2–10^4), have led to conclusions with controversy. Some studies [12 and 15] claimed that corrugated wings produced higher lift and comparable drag than that of its profiled counterparts. Some recent investigation [22, 23, 26, and 27] investigated corrugated airfoils which produces comparatively higher lift coefficients over the baseline airfoil at all angles of attack; these observations are different from the results reported by [12] where their smooth conventional airfoil shows higher lift coefficient than the corrugated airfoil. Skote [24] computationally investigated the boundary layers and the existence of the span wise flow in the corrugated airfoils and observed that the drag could be reduced by creating oscillation of spanwise flow. The present work is a further extension of that by Tamai et al [19] where flow separation and flow reversal were experimentally observed. The computational and experimental results [20, 21, 28-32] have revealed the spanwise induced flow, which shows the three dimensional behaviour of the airflow. However, the flow direction of the fluid [21 and 22] differs from the study [28] as the later showed the flow from tip to root. Flow separation occurs when the boundary layer thickness exceeds critical value which results in the adverse pressure gradient (APG). Flow separation occurs when the boundary layer travels far enough against an adverse pressure gradient that the speed of the boundary layer relative to the object falls almost to zero. The fluid flow becomes detached from the surface of the object, and instead takes the forms of eddies and vortices. The effect of an APG is to decelerate the flow near the body surface. This APG causes axial velocity to decrease in the direction of the stream lined (chord wise). Separation requires that the flow near the boundary stagnates; this occurs when flow actually reverses. Further, the flow characteristic about different spanwise location of the corrugated wing, and experimental boundary layer measurements which results in the flow separation and flow reversal were not conducted in previous research work. These flow characteristics will directly influence the wing aerodynamic performance, stall behaviour and flight stabilities. The current work aims to experimentally examine the spanwise flow quality of a gliding bio-inspired corrugated wing and compare the results with flat plate of the same chord, surface area and aspect ratio. The flow reversals of the both tested wings were visualized by using tufts and compared with each other. The boundary layers were measured at different wing semi span locations (30%, 60% and 90%), different Re_c and angles of attack in a low speed wind tunnel with fixed chord location (0.7 x/c). The results demonstrate that the spanwise flow occur from wing tip to root. The flow visualization and boundary layers study gave a clear distinction of flow separation and reversal phenomena of two tested wings.

2. METHODOLOGY

Two different wing models were used in the present study: (1) Flat plate and (2) Corrugated A wing. Both wing models have the same projected planform area (S), mean chord length (c) and aspect ratio (AR); details are given in table 2. The detailed wing geometries and fabrication methods are described in section 2.1, the experimental setup in section 2.2, and mathematical formulations in section 2.3.

2.1 Geometries and fabrication of wings

Numerous mock-ups of wing corrugated profiles have been proposed by many investigators. In the present study, the mid-section of the dragonfly forewing was selected for investigation, which was taken from Kesel Profile 2 [14] and the Murphy profile [25]. As a baseline comparison case, the flat plate of the same planform area, chord length and aspect ratio was selected.

These airfoils were selected because the Kesel and Murphy's corrugated profiles were used in many previous works [21-27].

The shape of the corrugation of dragonfly wings varies in spanwise direction. Kesel gained test profiles by taking photographs from three positions of a dried dragonfly forewing.

The present corrugated A wing, coordinates were generated (Table 1) and profile were made by MATLAB (Fig. 1), and CAD models of flat plate and corrugated A wing (Fig. 2).

The models were made of 2 mm thick aluminum sheet and manufactured by using micro bending machine of span 0.60m and chord of 0.12m which gives an aspect ratio of 5; full geometric details are given in table 2 and the manufacturing process is illustrated in figure 3.

The tufts were made of light wool of three different colours (black, green and red) so that they can be clearly identified and were glued on the upper surface near the trailing edge of the flat plate and corrugated A wing at the 30%, 60% and 90% of the semi span towards the right side of the wing.

Table 1. Coordinates of corrugated A profile

Lower surface		Upper surface	
x/c	y/c	x/c	y/c
1.00	0.000	0.000	0.00
0.908	0.000	0.010	0.033
0.856	0.000	0.096	0.017
0.684	0.029	0.191	0.046
0.610	0.000	0.263	0.017
0.558	0.029	0.335	0.046
0.394	0.000	0.394	0.017
0.335	0.029	0.558	0.046
0.263	0.000	0.610	0.017
0.191	0.029	0.684	0.046
0.096	0.000	0.856	0.017
0.010	0.017	0.908	0.017
0.000	0.000	1.000	0.000

Table 2. Geometric parameters of tested wing profiles

Profile	chord [m]	Thickness [m]	Span [m]	Planform area [m^2]	Aspect Ratio	Thickness /chord [%]
Flat plate	0.12	0.002	0.6	0.072	5	1.7
Corrugated A	0.12	0.0055	0.6	0.072	5	4.6

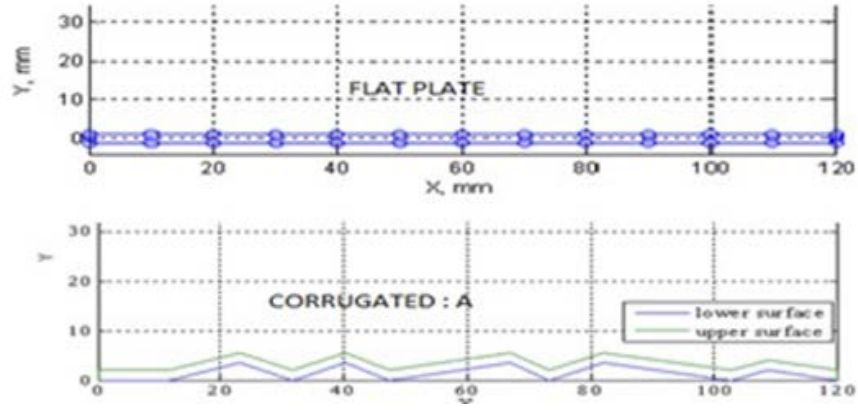

Figure 1. Geometry of flat plate and a corrugated A wing

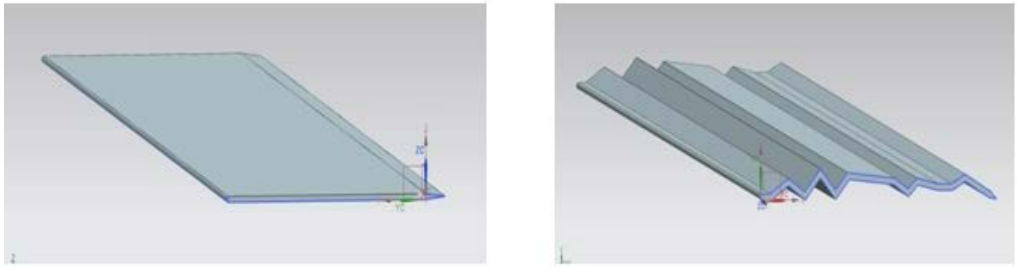

Figure 2. CAD model of flat plate and corrugated A wing [14]

Figure 3. Wing manufacturing process

2.2 Experimental setup

The low speed subsonic open circuit wind tunnel facility was used for the present experimental work. It has three main sections, an inlet, a test section and a diffuser at the exit of the tunnel. This wind tunnel has a test section size of 0.6 m × 0.6 m × 2 mand generates a maximum free stream velocity of 50 ms^{-1}. The contraction ratio is 9:1, contraction length 1.8 m, settling chamber size is1.8 m × 1.8 m, honey comb size 0.0 25 m × 0.0 25 m × 0.200 m. Two stainless steel screens of 8 meshes and 16 meshes are used to give minimum turbulence (less than 1% as claimed by the manufacturer) of the wind in test section. The smoke rake provided in contraction cone just before the test section which was used for smoke flow visualization. Velocity and pressure distribution was measured by the inclined tube manometer. The two limbs of the manometer are connected to the static pressure holes, one in the settling chamber just before contraction side and the other to that at the start of the test section. The reading in the manometer is approximately the dynamic head of the fluid in the test section and it serves as the reference for keeping the tunnel speed constant. The

inclination of the manometer is kept at 30^0 to the horizontal; at this angle the liquid (alcohol) column length change is twice to the vertical head, which gives superior accuracy. The tunnel is also provided with a Pitot-static tube, which can be traversed across the tunnel section. The fan is connected with a variable speed motor, which is varied by an AC controller and the motor required three phase power source. The experimental setup is illustrated in reference [29]. Both types of the wing models were fastened inside the test section to measure the boundary layers and also to visualize the flow. The wind tunnel is able to operate with minimum free stream velocity of $3ms^{-1}$to maximum $50ms^{-1}$. The angle of attack can be varied from -20^0 to $+20^0$ with accuracy of $\pm 0.5^0$; however in the present work the exact AOA were measured by using digital inclinometer with accuracy $\pm 0.1^0$**.**

2.3 Mathematical formulations

The lift and drag coefficient for the standard airfoil specimens by [24] can be found using Eq. (1) & Eq. (2), respectively.

$$C_L = L/(0.5\rho U^2 S) \tag{1}$$

$$C_D = D/(0.5\rho U^2 S \tag{2}$$

where ρ is the fluid density, U is the free stream velocity and S is the planform area, the coefficients of total lift is denoted by C_L and the total drag is denoted by C_D. They are obtained using the pressure coefficient between the upper and the lower surfaces for the airfoils. The normal and tangential force coefficients are given by Eq. (3) and Eq. (4), respectively.

$$C_L = C_n \cdot cos\,\alpha - C_t \cdot sin\,\alpha \tag{3}$$

$$C_D = C_n \cdot sin\,\alpha + C_t \cdot cos\,\alpha \tag{4}$$

Aerodynamic performance of a wing during gliding can therefore be determined by Eq. (5)

$$\in_R = C_L/C_D \tag{5}$$

3. RESULTS AND DISCUSSIONS

3.1 Tuft flow visualization

Flat plate tuft flow visualization was carried out in low speed wind tunnel by putting three different coloured tufts, black tuft which was fixed at 30% of semi span (BT30), green tuft which was fixed at 60% of semi span (GT60) and red tuft which was fixed at 90% (RT90) near the tip of the wing. The experiment was carried out at chord Reynolds number (Rec) ranging from $1.5x10^5$ to $3.75\ x10^5$, and angles of attack (AOA) ranging from - 2^0 to $+12^0$. At lower AOA from -2^0 to $+4^0$ angles of attack and with tested Reynolds numbers, the red tuft fixed at the wing tip (RT90) shows more fluctuation than other two tufts (BT30 and GT60), the green and black tuft behaviour was almost same. This phenomenon of flat plate flow found changed as the AOA increased to 6^0 and Re_c increased to 2.25×10^5 corresponds to 30 ms^{-1} of wind speed. The black tuft (BT30) fitted at the 30% of the wing semi span (near the wing root), started fluctuating sternly and came towards upper surface of the flat plate opposite to the direction of the free stream flow (-*x* direction). This indicated that the flow reversal took place first near the wing root due to adverse pressure gradient occurred between the upper and the lower surface. The upper surface pressure found to be lesser than

the lower surface of the wing and flow was taking place from lower side to upper side (Figure 4). The corrugated A wing at 6^0 AOA and same Re_c, the black tuft at 30% span was fluctuating severely but not reversing (Fig. 5). This clarify that the flow separation and reversal first encountered in a flat plate at the wing root at 6^0 AOA. However, the mid and tip tufts found to be stable and no flow reversal observed at this condition (Fig. 4 & 5). At this Re_c and AOA, the corrugated wing did not show any flow reversal. At angles of attack 10^0 and Re_c 2.25×10^5, both black and the green tufts (BT30 and GT60) which were fitted on both flat and corrugated wings were reversed upwards. The same qualitative results were shown by Chen and Skote [21], Skote [20, 25] and Ho and New [22], however their Reynolds number was one order lesser than the present study. It was also observed during experimentation that the reversal of the flow on both the tested wings at 30% and 60% of the semi span was coupled with spanwise flow of both black and green tuft from wing tip towards the wing root. The same result was computationally observed by Skote [12]. This demonstrates that the flow separation and flow reversal first occurred near wing root at lower angles of attack and Reynolds number $2.25x10^5$on flat plate only, however the flow reversal phenomena occurred to flat plate and corrugated A wing at higher angle of attack ($>10^0$) with expanded span location up to 70% (Fig. 6 & 7). It was observed that as the AOA is increased at the same Re_c, more area of the span is affected by the flow separation and reversal (Fig. 6 & 7). This was also noted that the red tuft (RT90) fitted just near the wing tip on both types of tested wings shown insignificant fluctuations. There was no sign of any types of flow separation and flow reversal at all tested angles of attack and Reynolds number (Fig. 4-7).

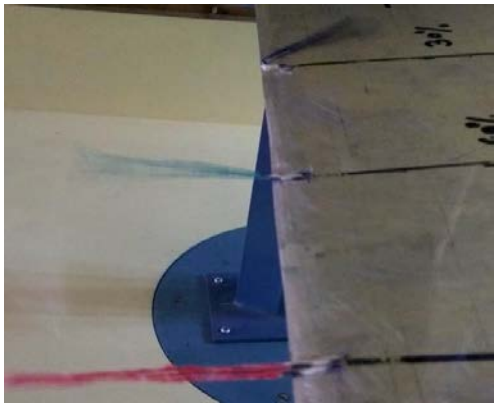

Figure 4. Flat plate tuft at 6^0 AOA, Re_C 2.25×10^5

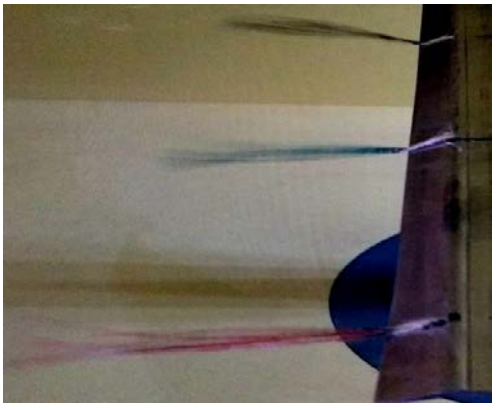

Figure 5. Corrugated A wing tuft at 6^0 AOA, Re_C 2.25×10^5

Figure 6. Flat plate tuft at 10^0 AOA, Re_C $2.25x10^5$

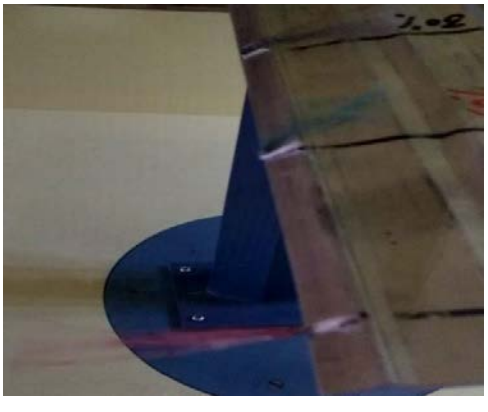

Figure 7. Corrugated wing tuft at 10^0 AOA, Re_C $2.25x10^5$

3.2 Boundary layer measurements

In Sec. 3.1, the qualitative tuft flow visualization and its analysis were undertaken to discover the flow reversal and flow separation. However, to find exactly the reason which causes flow separation and reversal, the measurement of boundary layers velocity profiles were done. The aim of the boundary layers measurement was to evaluate the velocity profile above the both tested wing surface at 70% of chord length (0.7 x/c) and at three different span locations i.e. 30%, 60% and 90% from the centre of the wing. The velocity profile was measured using twenty probes boundary layer measuring rake. The probes are connected to the manometer filled with alcohol aligned vertically on the profile. The velocity field around the wing surface creates the pressure difference between upper and the lower surfaces, which is responsible for producing the aerodynamic forces like lift and drag. These aerodynamic forces enable the object to fly in the air. The flow behaviour is governed by the parameters like AoA, thickness of profile, chord length, chamber and relative velocity across the surface of profile which often result in turbulent flow separation and flow reversals. In the present measurement campaign, a 20 probe boundary layer measuring rake along with multi tube manometer was fixed using transparent tubes and steel unions. In this rake, the number one probe (bottom most) is the first probe which is just touching the wing, representing the no slip condition and number twenty is the farthest from the wing, the distance between first probe to last probe is 35 mm. The boundary layers were measured in chord Reynolds numbers ranging from 1.5×10^5, 2.25×10^5, 3.0×10^5 and 3.75×10^5 and angles of attack ranging from 0^5-12^5. However, the results of Reynolds number 2.25×10^5 are given in this work as in this condition flow reversal is clearly visible. The comparison results of velocity profile probe number probe numbers are shown in figures 8-10. At 4^0 AOA and Re_c 2.25×10^5 the difference in velocity profile of flat plate at 30 % and 60 % of the semi span was found to be 10 ms^{-1} up to probe number 5 which has 4.5 mm boundary layer thickness. For corrugated wing, the difference between 30% and 60% of semi span was trivial i.e. 2 ms^{-1}. The difference in velocity profile of flat plate and corrugated A wing at 30% of semi span was found 5 ms^{-1}, and at 60% span the difference in velocity profile was only 3 ms^{-1} (Fig. 8). Further the flat plate velocity profile at 30% of wing span remained higher in comparison with corrugated A wing till probe number 12 (boundary layer thickness of 16.5 mm). However, the velocity profile of flat plate at 60% of span location was found to be the least among all (Fig. 8). In this condition no flow reversal was observed, however the severe fluctuation in 30% span location was observed. At 6^0 AOA and Re_c 2.25×10^5 the velocity profile difference of flat plate at 30% and 60% of semi span was found to be huge approximately 6 ms^{-1} up to probe number 5. For corrugated A wing, the difference between 30% span and 60% span was quite less approximately 3 ms^{-1}. The difference in velocity profile of flat plate and corrugated A wing at 30% of span was found 11 ms^{-1}, and at 60% span the difference in velocity profile was only 9 ms^{-1} (Fig. 9). Further the flat plate velocity profile at 30% of wing span remained much higher and velocity profile was found 41 ms^{-1}in comparison with corrugated A wing which was found 10 ms^{-1} (a difference of 31 ms^{-1} till probe number 10 (thicker boundary layer). This high velocity gradient cause very low pressure at 30% of semi span location and adverse pressure gradient occurred. This is the principal cause for creating the flow separation and flow reversal. Similar result was observed by tuft flow visualization as mentioned above and the flow visualization is validated by the measurements. The corrugated A wing velocity profile was found very less in comparison with flat plate beyond probe number 5 (a thin boundary layer) and hence no flow separation and flow reversal was observed. In this condition flow reversal was observed

in flat plate at 30% of span (Fig. 8). For 10^0 AOA and Re_c 2.25 × $10^5$the flat plate and the corrugated A wing at 30% and 60% of span, the velocity profile was found significantly high up to probe number 13 (boundary layer thickness 18.5 mm).

The flow separation and reversal was transpired up to 80% of the semi span on both types of the wings except tip of the wing (Fig. 10).

Similar result was given by the [13, 21, and 22]. At this AOA (10^0) and Re_c 2.25 x 10^5 the complete wing is in stall, which may cause the sudden loss of lift and falling of the aircraft.

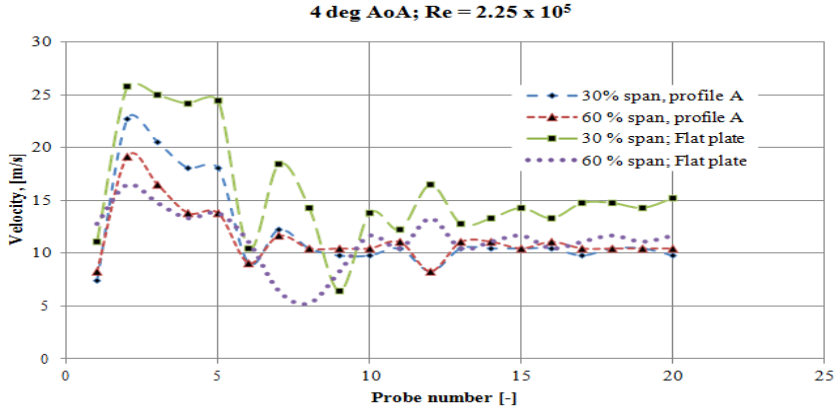

Figure 8. Comparison of boundary layer velocity at 4^0 AOA and Re_C 2.25×10^5

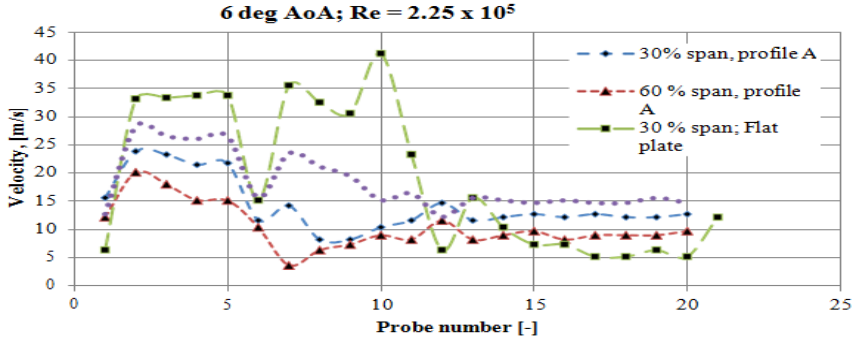

Figure 9. Comparison of boundary layer velocity at 6^0 AOA and Re_C 2.25x10^5

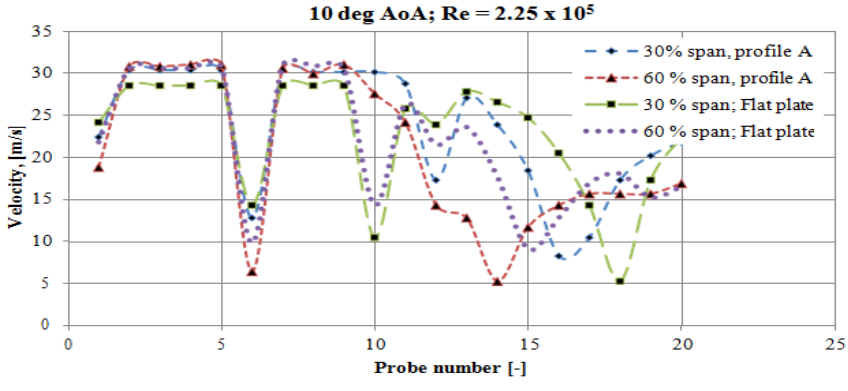

Figure 10. Comparison of boundary layer velocity at 6^0 AOA and Re_C 2.25x10^5

3.3 Analysis of spanwise flow of the corrugated wing

The spanwise flow of air combined with chordwise flowing air, changes the flow speed and direction. This creates a twisted flow and generates vortices. This causes generation of the additional induced drag on the wing. Past studies [11-15] on the wing corrugations claimed that 2-D studies was sufficient as there was no velocity parallel to the wing span and no intrinsic three-dimensionality effects. However, the 3-D experiments or computational simulations were limited to wing sections using uniform corrugation throughout the wing span. Hence, there was no change in model thickness or leading edge orientation in the spanwise direction. Chen and Skote [21] observed 3-D flow with strong spanwise flow from root to tip at 10^0AOA at Re_c1400. Hord and Lian [13] have conducted studies on the suitability of a 2-D simulation for the gliding corrugated wing. They tested a 3-D corrugated wing over a range of angles of attack from 0-12^0, and concluded that there was no spanwise flow and the difference of coefficients of forces between 2-D and 3-D cases were marginal, and it was due to variation of grid generation between 2-D and 3-D. The present study showed that there exist strong spanwise flows in the modeled flat plate and corrugated wing in same range of angles of attack. Chen and Skote [21] speculated that the spanwise variation, such as the changes in the orientation of the leading edge along the wing span, is the underlying cause of this spanwise flow. However, in the present study, the orientation of the leading edge was same throughout the wing span in corrugated A wing and flat plate and the span wise flow is clearly observed at all angles of attack above 6^0 in flat plate and above 10^0 in corrugated A wing (Fig. 6 and 7). The direction of the spanwise flow observed from tip to root in both the wings at 10^0 AOA and $Re_c = 2.25\times10^5$.

4. CONCLUSIONS

At low angles of attack i.e. 6^0 and chord Reynolds number less than 2.25×10^5there were no flow separation and reversal observed in any of the tested wings. The flow separation and reversal of the flat plate occurred at 6^0 angles of attack compared to corrugate A wing in which the flow reversal was noticed at 10^0 AOA and also tufts started moving towards wing root after reversal. This result is found qualitatively similar to that obtained by Chen and Skote [21] and Ho and New [22] at the Reynolds number being one order lower than that in the present work. The location of the flow separation and reversal was observed first near the root i.e. 30% of the semi span for flat plate models. As the AOA increased to 10^0 or higher, flow reversal was also found in corrugated A wing and also in flat plate. Both black and green tufts reversed, indicated that the flow separation and reversal extend to more than two third parts (80% of total wing span) of the wings semi span.

The same result is predicted by [21]. The flow visualization demonstrated strong spanwise flow occurred in entire wing, moving from wing tip to wing root. The boundary layer velocity profile measurements confirmed that the boundary layer thickness at 10 degree angles of attack is higher comparing to lower angles of attack. The results showed that the corrugated A wing is delayed the stall and reduced flow separation and reversal from 6^0 in flat plate to 10^0 in corrugated A wing. The major advantage in corrugated wing is to extend safe flight envelop up to 40% extra AOA without stall. The corrugated wing can be used for Micro Arial Vehicles which fly in the range of tested Reynolds number. The boundary layer behaviour of corrugated A profile is found to be better than in the case of the flat plate which signifies that the corrugated A profile is more suitable for low speed and viscous flights which are commonly observed in natural flying avian and insects.

REFERENCES

[1] Y. H. Chen, M. Skote, Y. Zhao, Dragonfly (*Sympetrum flaveolum*) flight: kinematic measurement and modelling, *Journal of Fluids and Structures*, **40**: 115–126. DOI:10.1016/j.jfluidstructs.2013.04.003, 2013.

[2] D. J. S. Newman, R. J. Wootton, An approach to the mechanics of pleating in dragonfly wings, *Journal of Experimental Biology*, **125**: 361–372, 1986.

[3] C. J. C. Rees, Aerodynamic properties of an insect wing section and a smooth aerofoil compared, *Nature*, **258**: 141–142, 1975a, DOI:10.1038/258141a0.

[4] C. J. C. Rees, Form and function in corrugated insect wings, *Nature*, **256**: 200–203, 1975b, DOI: 10.1038/256200a0.

[5] S. Sudo, K. Tsuyuki, J. Tani, Wing morphology of some insects, *JSME International Journal Series C-Mechanical Systems, Machine Element sand manufacturing*, **43**: 895–900, DOI: 10.1299/jsmec.43.895, 2000.

[6] R. J. Wootton, Function, homology and terminology in insect wings, *Systematic Entomology*, **4**: 81– 93, DOI:10.1111/j.1365-3113.1979.tb00614.x, 1979.

[7] R. J. Wootton, Support and deformability in insect wings, *Journal of Zoology*, **193**:447–468, DOI: 10.1111/j.1469-7998.1981.tb01497.x, 1981.

[8] R. J. Wootton, Functional morphology of insect wings, *Annual Review of Entomology*, **37**:113–140, DOI: 10.1146/annurev.en.37.010192.000553, 1992.

[9] A. K. Kesel, Aerodynamic characteristics of dragonfly wing sections compared with technical aerofoils, *Journal of Experimental Biology*, **203**: 3125–3135, 2000.

[10] M. Mingallon, S. Ramaswamy, The architecture of the dragonfly wing: a study of the structural and fluid dynamic capabilities of the ansoptera's forewing, in: *ASME International Mechanical Engineering Congress & Exposition*, Denver, Colorado, USA 11-17 November 2011.

[11] M. Okamoto, K. Yasuda, A. Azuma, Aerodynamic characteristics of the wings and body of a dragonfly, *Journal of Experimental Biology*, **199**: 281–294, 1996.

[12] A. Vargas, R. Mittal, H. Dong, A computational study of the aerodynamic performance of a dragonfly wing section in gliding flight, *Bio inspiration & Bio mimetic*, **3**: 1–13, DOI.org/10.1088/1748-3182/3/2/026004, 2008.

[13] K. Hord, Y. Lian, Numerical investigation of the aerodynamic and structural characteristics of a corrugated airfoil, *Journal of Aircraft*, **49**: 749–757, http://dx.doi. org/ 10. 2514 /1. C031135, 2012.

[14] A. B. Kesel, U. Philippi, W. Nachtigall, Biomechanical aspects of the insect wing: an analysis using the finite element method, *Computers in Biology and Medicine* **28**: 423–437, https://doi.org/10.1016/S0010-4825(98)00018-3, 1998.

[15] W. K. Kim, J. H. Ko and H. C. Park, et al. Effects of corrugation of the dragonfly wing on gliding performance, *Journal of Theoretical Biology*, **260**: 523–530, DOI:10.1016 /j. jtbi. 2009, 07.015, 2009.

[16] Y. Lian, T. Broering, K. Hord, The characterization of tandem and corrugated wings, *Progress in Aerospace Sciences* **65**: 41–69, https://doi.org/10.1016/j.paerosci.2013.08.001, 2014.

[17] J. M. Wakeling, C. P. Ellington, Dragonfly flight. I. Gliding flight and steady-state aerodynamic forces, *Journal of Experimental Biology*, **200**: 543–556, PMID: 9318238, 1997.

[18] A. Obata, S. Sinohara, Flow visualization study of the aerodynamics of modeled dragonfly wings, *AIAA Journa*l, **47**: 3043–3047, http://dx.doi.org/10.2514/1.43836, 2009.

[19] M. Tamai, Z. Wang, G. Rajagopalan, et al., Aerodynamic performance of a corrugated dragonfly airfoil compared with smooth airfoils at low Reynolds numbers, In: *Proceedings of the 45thAIAA Aerospace Sciences Meeting and Exhibit*, Reno, Nevada, pp 1-12.DOI/abs/10.2514/6.2007-483, 8-11 January 2007.

[20] M. Skote, Scaling of the velocity profile in strongly drag reduced turbulent flows over an oscillatingwall, *I. J of Heat and Fluid Flow*, **50**: 352–358, https://doi.org/10.1016 /j.ijheatfluidflow.2014.09.006, 2014.

[21] Y. H. Chen, M. Skote, Gliding performance of 3-D corrugated dragonfly wing with spanwise variation, *Journal of Fluids and Structures*, **62**: 1-13, https://doi.org/10.1016 /j. j fluid structs, 2015.12.012, 2016.

[22] W. H. Ho, T. H. New, Unsteady numerical investigation of two different corrugation airfoils, *Proc IMechE Part G: J Aerospace Engineering*, **0**: 1–15, DOI/abs/ 10.1177 / 095441001668 2539, 2016.

[23] W. H. Ho, T. H. New, CFD Analysis of Bio-Inspired Corrugated Aerofoils, In: *Proceedings of Eleventh International conference of Fluid Dynamics*, Alexandria, Egypt, 19-21 December 2013.

[24] M. Skote, Turbulent boundary layer flow subjected to stream wise oscillation of Spanwise wall-velocity, *Physics of Fluids*, **23**:1701-1704, DOI: http://dx.doi.org /10.1063 /1. 3626028, 2011.

[25] J. Murphy, H. Hu, An experimental study of a bio-inspired corrugated airfoil for micro air vehicle applications, *Exp Fluids*, **492**: 531–546, DOI:10.1007/s00348-010-0826-z, 2010.

[26] T. J. Flint, M. C. Jermy, T. H. New, W. H. Ho, Computational study of bio-inspired corrugated airfoil, *I. J. of heat and fluid flow*, **65**: 328-341, DOI: http://dx.doi.org/10.1016/ j. int. journal of Heat and Fluid flow.2016.12.009, 2017.

[27] W. H. Ho, T. H. New and E. Matare, Unsteady CFD analysis of an oscillating Aerofoil inspired by dragonfly wings, In: *Proceedings of Topical Problems of Fluid Mechanics*, Prague, paper no- 021, DOI: https://doi.org/ 10.14311 /TPFM.2017.021, 15-17 February 2017.

[28] Y. D. Dwivedi, V. Bhargava, P. M. V. Rao, D. Jagadish, Aerodynamic Performance of Micro Aerial Wing Structures at Low Reynolds Number, *INCAS Bulletin*, **11** (1): 107-120, DOI:10.13111/2066-8201.2019.11.1.8, 2019.

[29] Y. D. Dwivedi, W. H. Ho, D. Jagadish, and P. M. V. Rao, Spanwise Flow Analysis of Gliding Bio-inspired Corrugated Wing, *Journal of Advanced Research in Dynamical & Control Systems*: **12**-Special Issue, August 2017.

[30] Y. D. Dwivedi. V. Sridhar, P. M. V Rao, D. Jagadish, Computational Study of Fluid Flow Behaviour Over Bio-Inspired Corrugated Airfoil for Micro Aerial Vehicles, *International Conference on Advances in Thermal Systems, Materials and Design Engineering (ATSMDE 2017)*, VJTI Mumbai, https://dx.doi.org/ 10.2139/ ssrn.3101272, Dec 2017.

[31] Y. D. Dwivedi, V. Bhargava, Aerodynamic Characterization of Bio inspired Wing, *MOJ APP Bio Biomech*, **3** (1): 1-10, 2019.

[32] V. Sridhar, Y. D. Dwivedi, *Effects of Peak Shape in Bio Inspired Corrugated Wing*, International Conference on Advances in Thermal Systems, Materials and Design Engineering (ATSMDE 2017), VJTI Mumbai, https://dx. doi.org/ 10. 2139/ ssrn. 3101316, Dec 2017.